

## Energy Storage Design Considerations for an MVDC Power System

L. J. Rashkin<sup>1</sup>\*, PhD. EE, J. C. Neely<sup>1</sup>, PhD. EE, D. G. Wilson<sup>1</sup>, PhD. EE, S. F. Glover<sup>1</sup>, PhD. EE, N. Doerry<sup>2</sup>, PhD. , S. Markle<sup>2</sup>, T. J. McCoy<sup>3</sup>, PhD.

<sup>1</sup> Sandia National Laboratories, Albuquerque, NM, USA

<sup>2</sup> NAVSEA, PMS 320, Washington, D.C., USA

<sup>3</sup> McCoy Consulting, Box Elder, ND, USA

\* Corresponding Author. Email: lrashki@sandia.gov

### Synopsis

As part of the U.S. Navy's continued commitment to protecting U.S. interests at home and abroad, the Navy is investing in the development of new technologies that broaden U.S. warship capabilities and maintain U.S. naval superiority. In particular, NAVSEA is supporting the development of power systems technologies that help the Navy realize an all-electric warship. It is recognized that a challenge to fielding an all-electric power system architecture includes minimizing the size of energy storage systems while maintaining the response times necessary to support potential pulsed loads. This work explores the trade-off between energy storage requirements (i.e. size and weight) and performance (i.e. bandwidth and storage) in the context of a power system architecture that meets the needs of the US Navy.

To compare energy storage technologies and appropriately size them, it is necessary to specify size and weight requirements and thus consider the energy density of the technology in Wh/kg and specific power density in W/kg. The modelled time domain behaviour for different load types and control delays were used to determine technology and sizing requirements by comparing the total energy and maximum power used in the simulation to a Ragone plot. Simulation results based on operational vignettes were used to identify a range of specific power and energy densities that will meet system requirements. Potential energy storage sizing can be determined by approximating where a selected technology intersects with the energy and power requirements of the system.

Another major component necessary to determine energy storage technology is the frequency domain behaviour of the system. In this work, the energy storage control bandwidth is evaluated in simulation for different loading scenarios, and a trade-off between size/weight and response bandwidth is illustrated.

*Keywords:* Energy Storage; Frequency Response; Control; Integration; Pulsed Loads

### 1. Introduction: Energy storage and medium voltage DC power

Controls are recognized as a primary challenge to fielding a medium voltage DC (MVDC) power system for future Navy ships. The service power demands of these future naval warships may include advanced mission systems which need large amounts of power in short pulses (Doerry, 2007). To support these pulse power loads, transient response times will need to decrease significantly from what is available today from gas turbine and diesel driven generators (Doerry, 2007). The goal of this project is to utilize advanced control design techniques (Robinett, 2011), (Wilson, 2012), (Wilson, 2014), (Wilson, 2015), (Weaver, 2016) to support and solve the development of Naval Power and Energy Systems (NPES) Technologies that will enable open architectures, help develop common component requirements, and create a design infrastructure to guide and support Navy and industry Research and Development (R&D) and Science and Technology (S&T) investments.

### 2. Model Development

The control architecture, analytical and simulation models, and hardware testbed described in this work were originally developed as part of a Grand Challenge Laboratory Directed R&D project at Sandia National Laboratories to develop secure, scalable, microgrid capabilities. The Secure Scalable Microgrid (SSM) is an innovative grid architecture that steps away from unidirectional power flow and limited information flow and adopts closed-loop controls and an agent-based architecture with integrated communication networks. With the addition of feedback components to the input signal, an intelligent power flow control is established that provides a basis for the integration of renewables and other distributed power sources into the electrical power grid (Robinett, 2011), (Wilson, 2012), (Wilson, 2014). This new approach enables self-healing, self-adapting, self-

organizing architectures that allow for trade-off considerations between storage in the grid and information flow that controls generation sources, power distribution, and load profiles. This approach extends to Navy ship applications with a focus on the stochastic nature of the pulse power mission loads rather than stochastic generation.

Introduction of this agent-based, distributed, nonlinear control to maintain reliable energy distribution, minimizes the need for excessive storage or backup generation (Wilson, 2012) and will be a revolutionary step toward high penetration of pulsed loads (advanced weapons and radar) in the all-electric warship. The development of analytical dynamic nonlinear source models, scalable agent-based architectures and multi-time variant simulations will be key components of this solution. The SSM distributed nonlinear dynamical models and control architectures will be employed as an initial starting point to address the NPES problem for future naval warships.

### 2.1. System layout

A reduced scale topological model of a shipboard power system (shown in Figure 1) was emulated physically on the SSMTB hardware and in simulation using a Simulink model library that was made to represent the SSMTB components. This configuration uses 3 networked direct current (DC) microgrids laid out to emulate a starboard, port, and bow bus for a ship architecture. The port and starboard buses, Microgrid 1 and 2, are functionally identical with a diesel generator, distributed energy storage, and a propulsion load each. The bow grid, Microgrid 3, has a service load, pulsed load, and energy storage. The three grids are connected using grid-to-grid power electronic converters to control the power flow between grids. All components interact with the grid through power electronics and a hierarchical control structure.

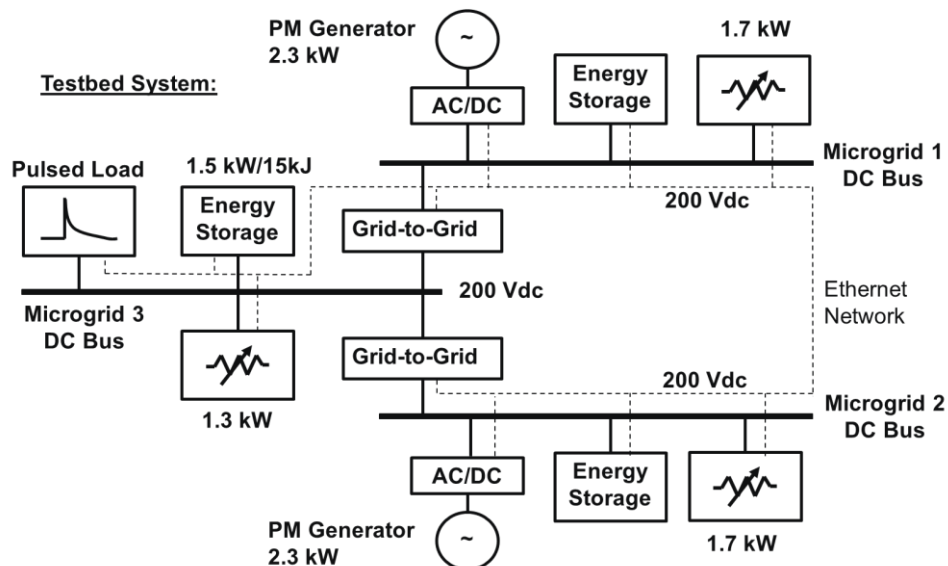


Figure 1: Scaled electric ship microgrid system.

### 2.2. Control Algorithm

A simplified dynamic optimization planner, based on a guidance control algorithm, was employed for investigation of all the multiple mission load scenarios. The multiple mission vignette-based load profiles (Stevens, 2015), (Chalfant, 2015) were realized and simulated with equivalent SSM load profiles. The guidance controller (Figure 2) provides regular updates to the power converters in the system. The generators and energy storage communicate current and voltage measurements. The guidance controller sends voltage references to the energy storage units which then regulate bus voltage. The guidance controller also sends power commands to the converters that connect generators to the bus. This involves computation of  $\lambda^*$ , the quasi-static value of the duty cycle of the upper switch in the boost converter which is equal to  $(1-D)$ , where  $D$  is the duty cycle of the boost converter switch. This is then used to compute the current command into the boost converter. Both require knowledge of the load power requirement. Power requirements are computed using a real-time load estimator and voltage set points.

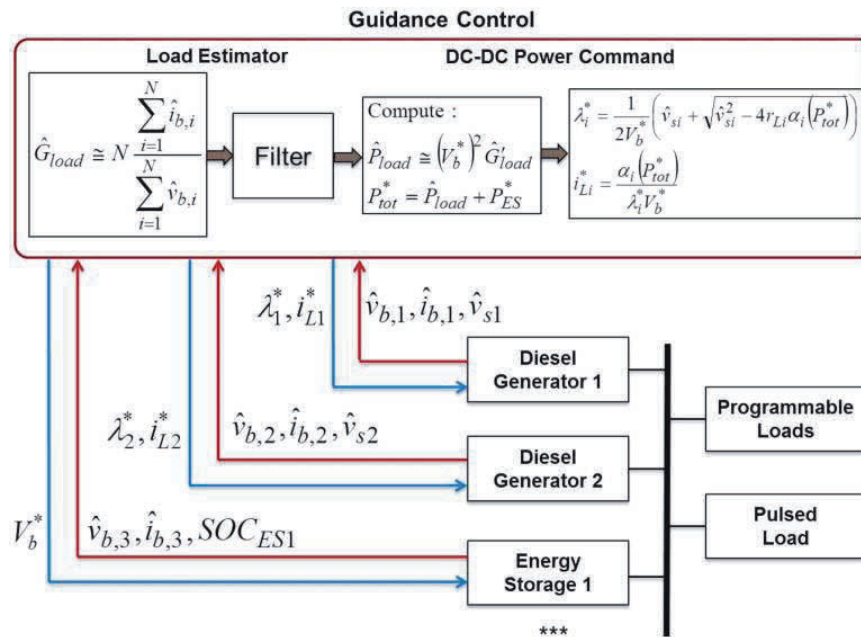


Figure 2: Guidance control strategy (simplified dynamic optimization planner)

### 2.3. Load Profiles

A literature review was performed in general to identify salient load characteristics; however, the operational vignettes of interest to the Electric Warship program described in references (Stevens, 2015), (Chalfant, 2015) were selected for further development. The vignette was decomposed into separate types of loading referred to as the propulsion load, service load, mission load #1, and mission load #2. These loads were inspected visually and implemented in MATLAB™ as shown in Figure 3. The vignette-based load profiles assumed a base voltage of 20kV DC and a base power of 80 MW; these profiles were then per-unit scaled to be compatible with the SSMTB power levels for a bus voltage of 200 Vdc and base power of 4.6 kW, which reflects the hardware capabilities of the system (Neely, 2016). Figure 4 shows the Vignette 1 power profile as scaled for the SSMTB.

### 2.4. Simulation results

To understand the impact of pulsed loads on the controls, four load cases based on the vignettes provided by (Stevens, 2015), (Chalfant, 2015) were defined. The first case used only the propulsion and service loads and is referred to as the No Mission Loads case. The second case added a 10 MW pulsed load from the vignette labelled Mission Load 1. The third case added a 700 kW pulsed load from the vignette labelled Mission Load 2. The final case, referred to as the All Mission Loads case, included both Mission Load 1 and Mission Load 2. Each load case was tested under different balances between generator response and energy storage response. This balance was varied by adjusting the time constant on a first order filter of generator power command. The filter used time constants of (1) 0.1356, (2) 0.5299, (3) 2.005, (4) 7.512, and (5) 28.56 seconds. The longer time constant moves the burden of supplying the loads more to the energy storage and the shorter time constant moves that burden more to the generation during transients.

Figure 5 shows the simulated bus currents in the All Mission Loads case with a time constant of 0.1356 seconds. While there is some response from the various energy storages, the generator is the primary supply for the pulsed loads. Similarly, the same load case having a time constant of 28.56 seconds, see Figure 6, shows that the energy storage response to the pulsed load is greater. This can also be seen by the generator speed response in Figure 7. With a time constant of 0.1356 seconds, the generator speed varies significantly from the reference speed and spikes in response to the pulsed loads. With a time constant of 28.56 seconds, the generator speed varies slowly and very little variation results from the pulsed loads.

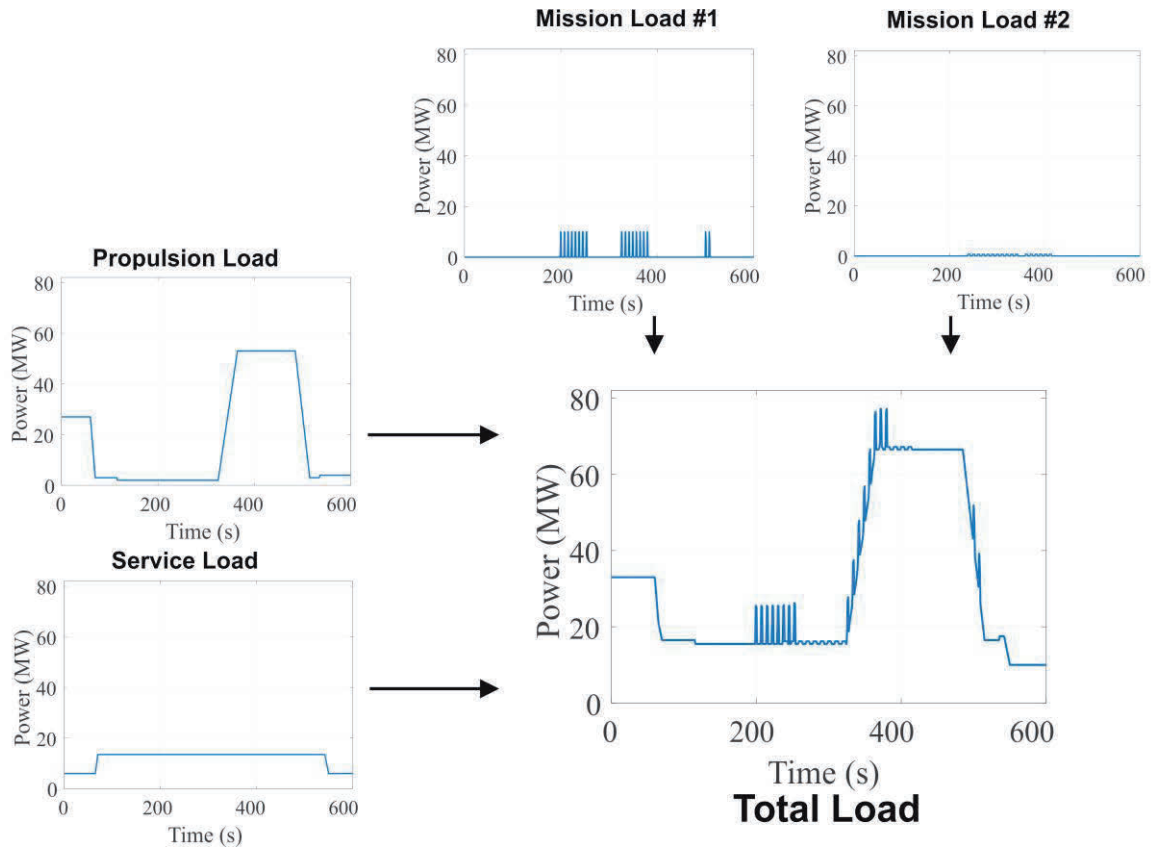


Figure 3: Decomposition of vignette 1 (Cramer, 2015)

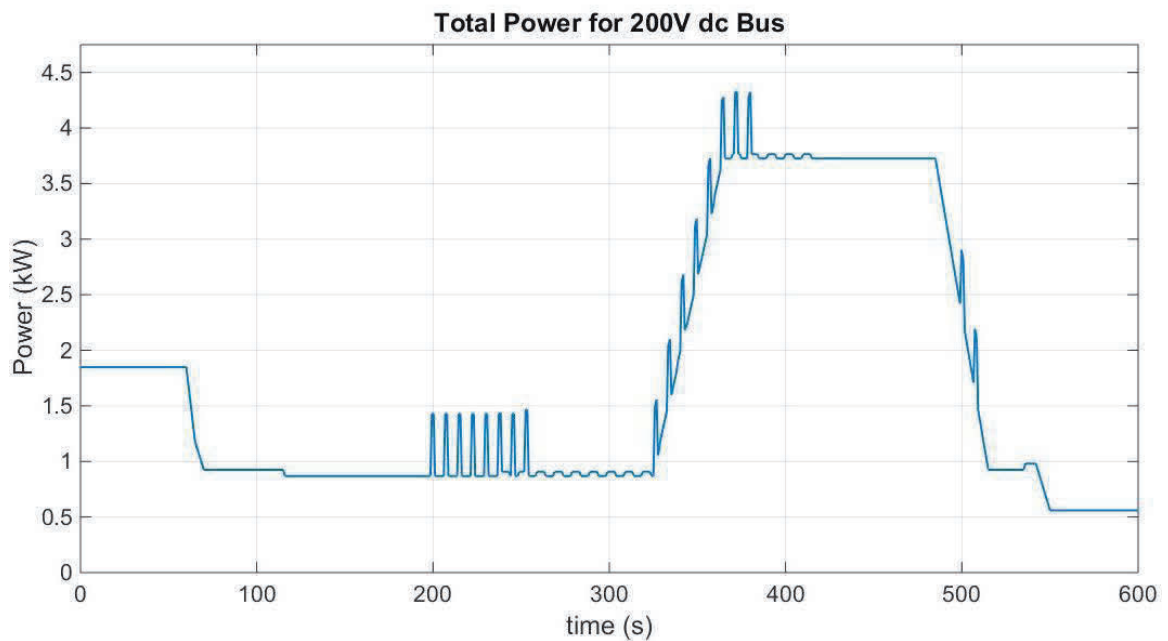


Figure 4: Scaled total power profile for SSMTB representing Vignette 1

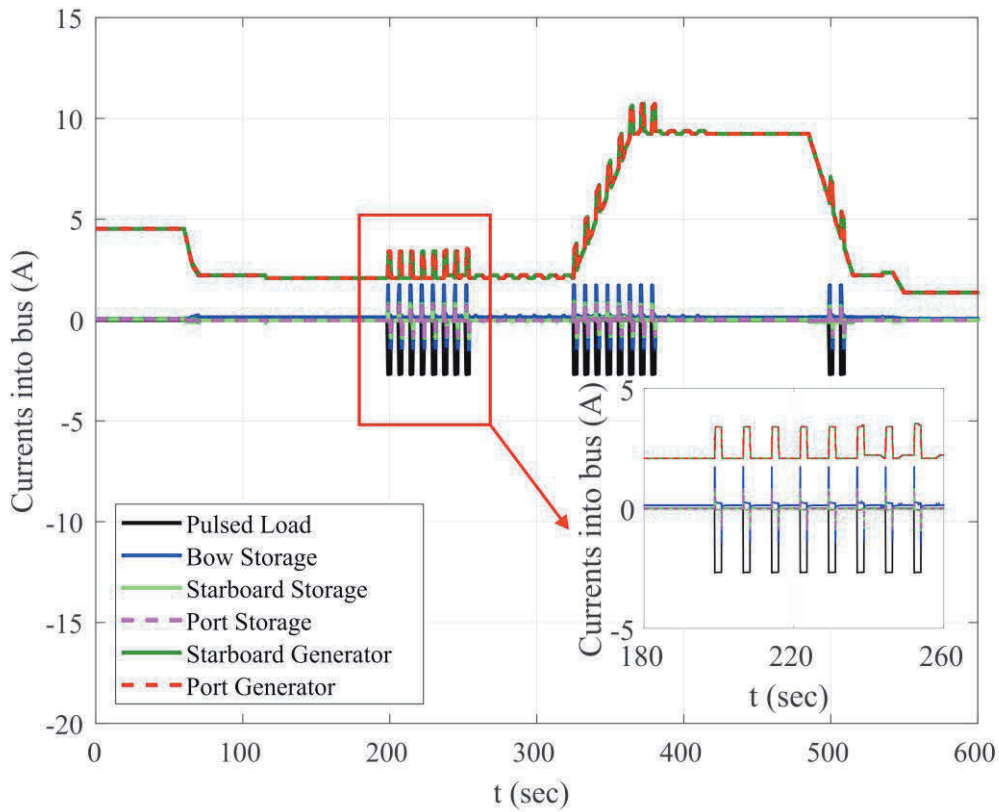


Figure 5: Bus Currents for All Mission Loads case with time constant of 0.1356 seconds

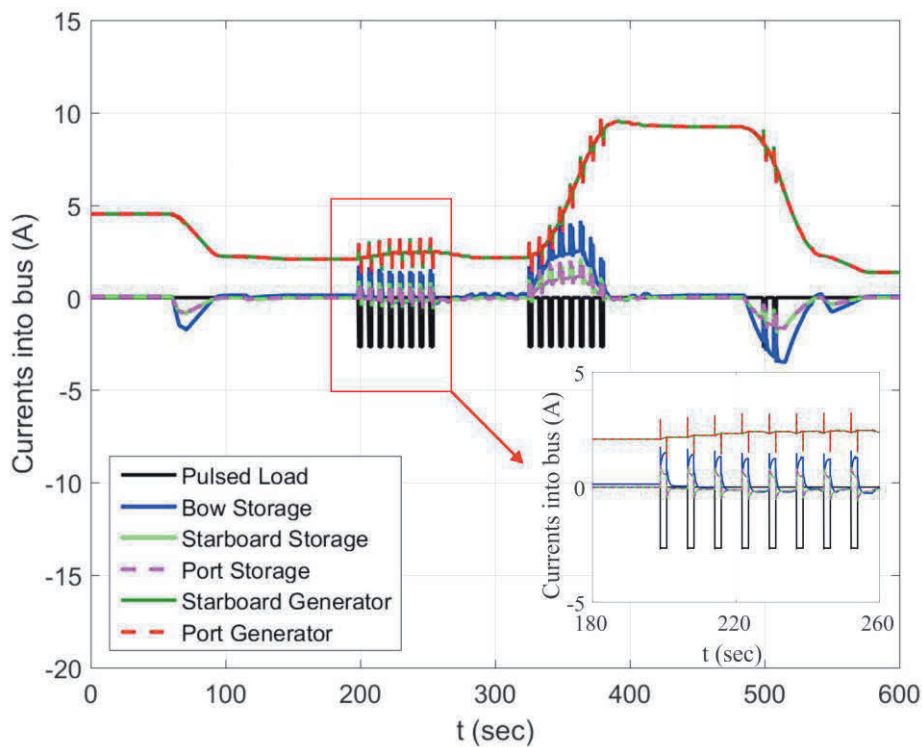


Figure 6: Bus Currents for the All Mission Loads with time constant of 28.56 seconds

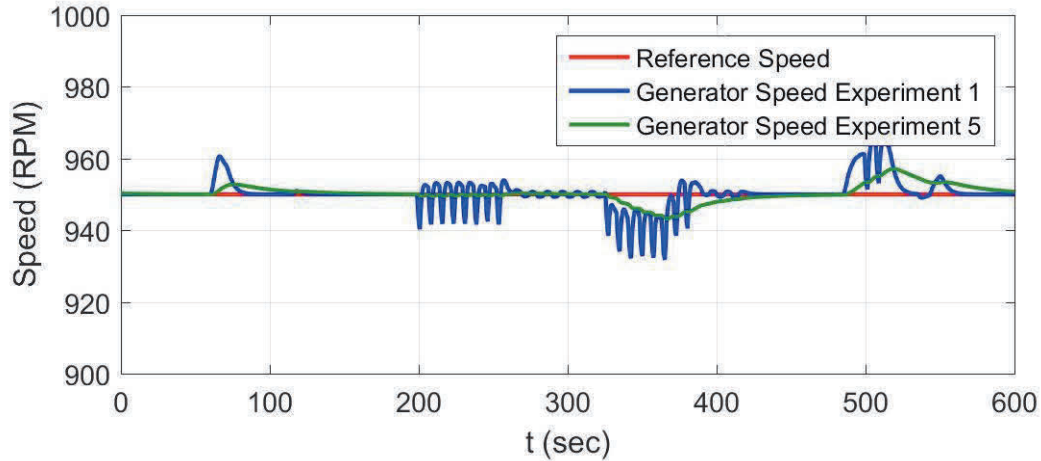


Figure 7: Comparison of generator speeds in All Mission Loads case

To help quantify the effect of the filter time constant on performance (Neely, 2015), a Pareto frontier was identified to investigate the trade-off between energy storage and generator control effort; the two performance quantities  $J_1$  and  $J_2$  are defined as

$$J_1 = \int_{t_0}^{t_f} \left( \sum_i^{N_{Gens}} (i_{bi}(\tau) - \hat{i}_{bi})^2 \right) d\tau \tag{3.1}$$

$$J_2 = \int_{t_0}^{t_f} \left( \sum_i^{N_{ES}} (i_{ESi}(\tau) - \hat{i}_{ESi})^2 \right) d\tau \tag{3.2}$$

where  $i_{bi}(t)$  are the currents delivered to the respective busses by the starboard and port generator converters as a function of time,  $N_{Gens}$  is the number of generators, and  $i_{ESi}(t)$  are the bus currents from the  $N_{ES}$  energy storage systems. The values  $\hat{i}_{bi}$  and  $\hat{i}_{ESi}$  represent the fast average taken over a 7 second period:

$$\hat{i}_{bi} = \frac{1}{T_{fa}} \int_{t-T_{fa}}^t i_{bi}(\tau) d\tau \tag{3.3}$$

$$\hat{i}_{ESi} = \frac{1}{T_{fa}} \int_{t-T_{fa}}^t i_{ESi}(\tau) d\tau \tag{3.4}$$

where  $T_{fa}$  is the period of the fast average. For the purposes of this simulation,  $T_{fa}$  was set to 7 seconds which is approximately equal to the period of the largest mission load.

Figure 8 shows the Pareto frontiers between generator control effort and energy storage control effort for the simulated results of All Loads cases. There is a clear trade-off between generator effort and energy storage effort for All Loads cases. This trade-off is also consistent between load cases. The addition of larger mission loads will increase the required total effort.

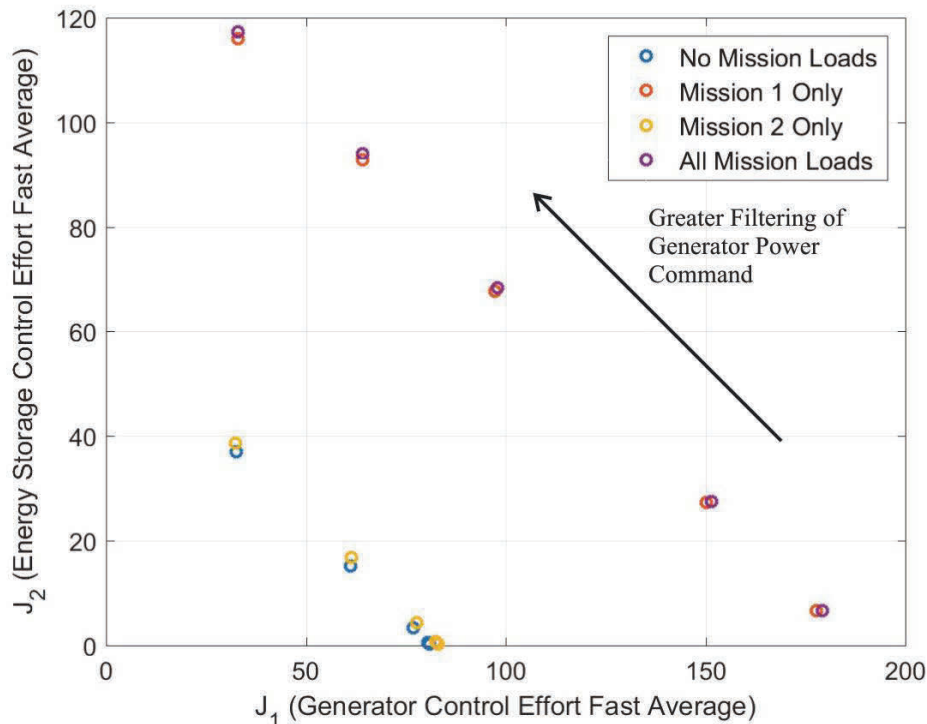


Figure 8: Comparison of Pareto Frontiers for All Loads cases

### 3. Energy Storage Sizing

#### 3.1. Power and energy requirements

The time domain results for the different load types and control delays were used to determine technology and sizing requirements by mapping the total energy and maximum power requirements computed in simulation to the Ragone plot (Byrne, 2007) assuming different energy storage system masses.

Figure 9 shows the power and energy requirements of the energy storage system on grid 3 to maintain the operational point. The energy storage system on bus 3 represents the highest requirements for power and energy, especially with the full vignette. In order to compare energy storage technologies and appropriately size them, it is necessary to find the specific energy density in Wh/kg and specific power density in W/kg requirements. Since mass is not considered by the simulation model, it was treated as a variable quantity. The worst case scenario, the all mission loads case on bus 3, was taken and the required power was divided by masses ranging from 10 kg to 100,000 kg. This results in a range of specific power and energy densities that will meet system requirements even in the worst case.

Figure 10 shows the results from a 20 kV system plotted against a Ragone plot (Byrne, 2007). The Ragone plot shows the energy and power densities of various generation technologies; by plotting the results of the simulation on top of this graph it is possible to see the necessary sizing of any potential solution. In Figure 9, the results scaled by potential mass that were calculated are plotted in black while the area of potential solutions is outlined in blue. Potential energy storage sizing can be determined by approximating where a selected technology intersects with this enclosed area and estimating the appropriate size with a comparison to the nearest pre-calculated values. These results indicate that an approximately 3000 kg flywheel would represent the minimum technology for the vignette.

#### 3.2. Frequency Analysis

The other major component necessary to determine energy storage technology is the frequency domain behaviour of the system. To analyse the frequency domain behaviour of the system, a chirp was applied in simulation to the load on microgrid 3 while all other loads were held at a constant level. The chirp signal is a sinusoid with a time varying frequency that allows for a large range of frequency content to be applied to a system, which allows for frequency domain quantification of a complex system. The load power of the load on microgrid 3 was then treated as the input to the system. The output powers of the diesel generators and energy storages were then recorded as the system outputs. The frequency domain behaviour of the input and outputs were then calculated using the MATLAB `fft()` function and the transfer function found by dividing each output by the input.

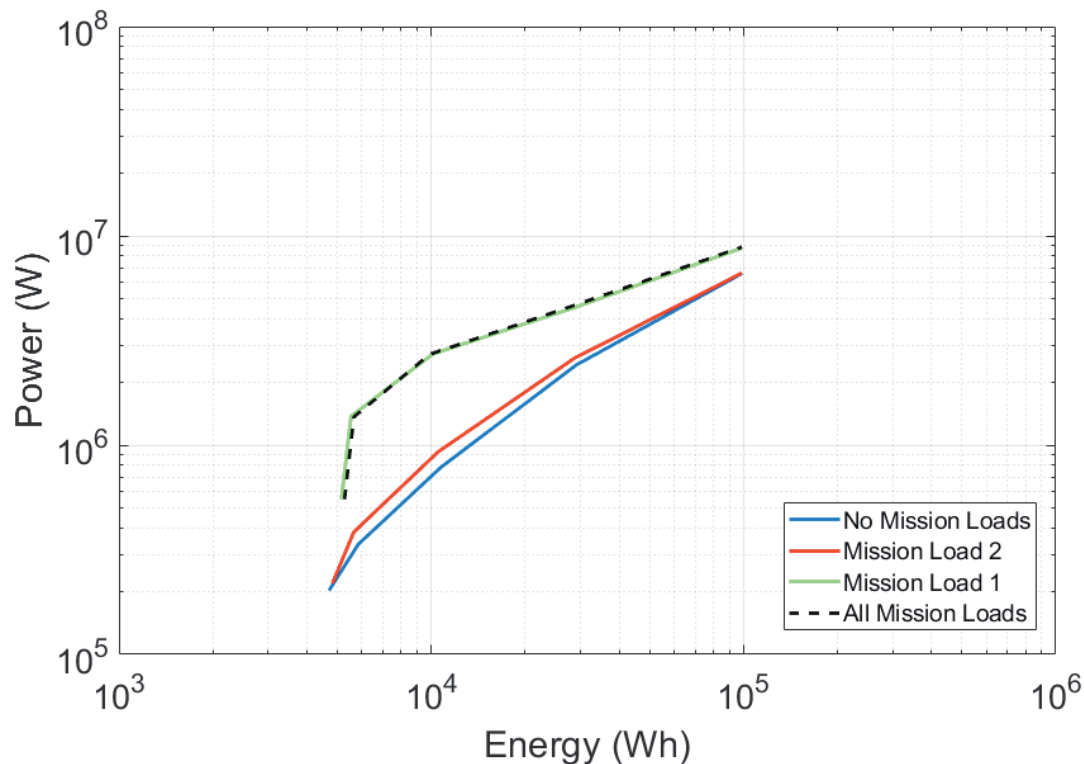


Figure 9: Required Power vs Required Energy for the ESS on Bus 3 for All Loads cases and time constants

The resulting transfer functions are shown in Figure 11 through Figure 13. Figure 11 shows the transfer function of the diesel generator on microgrid 1. Because of the symmetry of the system, the transfer function for the other diesel generator is equal to this graph, and is therefore omitted. As shown, for all filter constants the diesel generators will contribute to the low frequency behaviour of the system up until a cut off frequency is reached. As the filter's time constant is increased, the cut off frequency of the transfer function goes down. At very high frequencies the generators are only able to contribute a set amount of power to the system, and the transfer functions converge.

Figure 12 shows the transfer function for the energy storage on grid 1. Due to the symmetry of the system the transfer function for the energy storage on grid 2 will be equal to this and is omitted here. At low frequencies the energy storages will need to contribute more power to the system as the controller time constant increases to compensate for the diesel generators contributing less. As the frequency increases to 10 Hz, the contribution from the energy storages converges and the storages will always provide equivalent power to the system. Above 200 Hz the contribution from these energy storages becomes attenuated due to the grid-to-grid connections in the system filtering those frequencies out from what is delivered to the load on grid 3.

Figure 13 shows the transfer function between the grid 3 energy storage and load. Similar to the transfer functions of the other energy storages, at low frequencies the energy storages will need to contribute more power to the system as the controller time constant increase, but the transfer functions will converge at higher frequencies. Unlike the other energy storages, over 200 Hz the energy storage will have to contribute significantly more to the power demands of the load since it is the only energy source present on that bus.

These results show that even though the flywheel energy storage solution makes the most sense from an energy density and power density perspective, it might not be capable of supplying distributed pulsed loads by itself. According to (Snoussi, 2016), flywheels are most effective in the frequencies between 10 mHz and 100 mHz, so pulsed loads with frequency content in the Hz range and above will need to be supplemented with another type of energy storage or a hybrid energy storage solution.

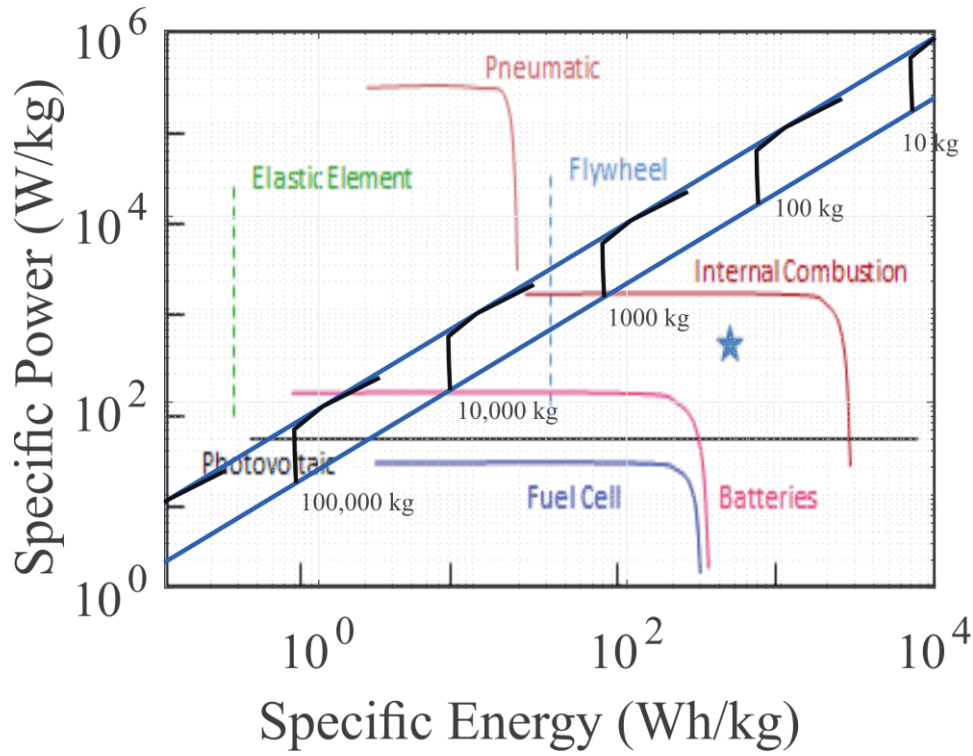


Figure 10: Energy Storage System requirements as a function of system size for the full sized system

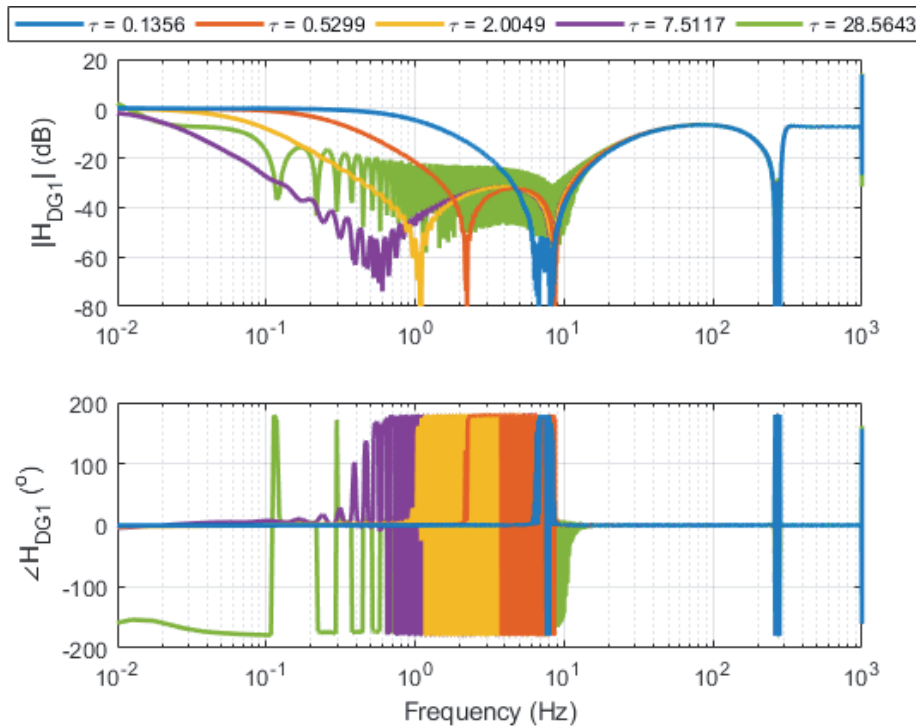


Figure 11: Transfer Function between the Diesel Generators and the Grid 3 Load

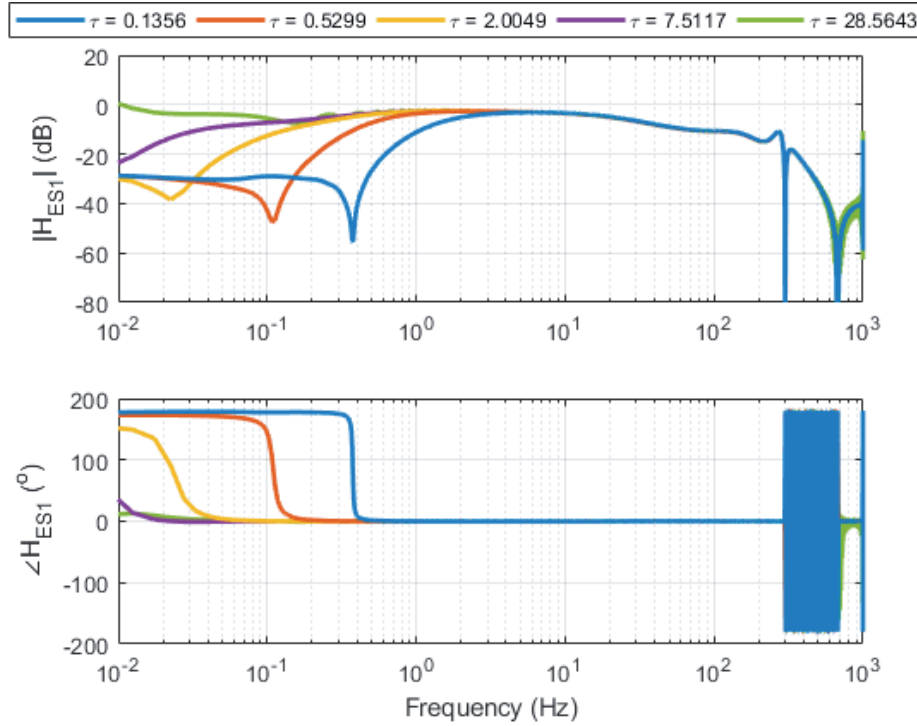


Figure 12: Transfer Function between Energy Storages on Grids 1 and 2 and the Grid 3 Load

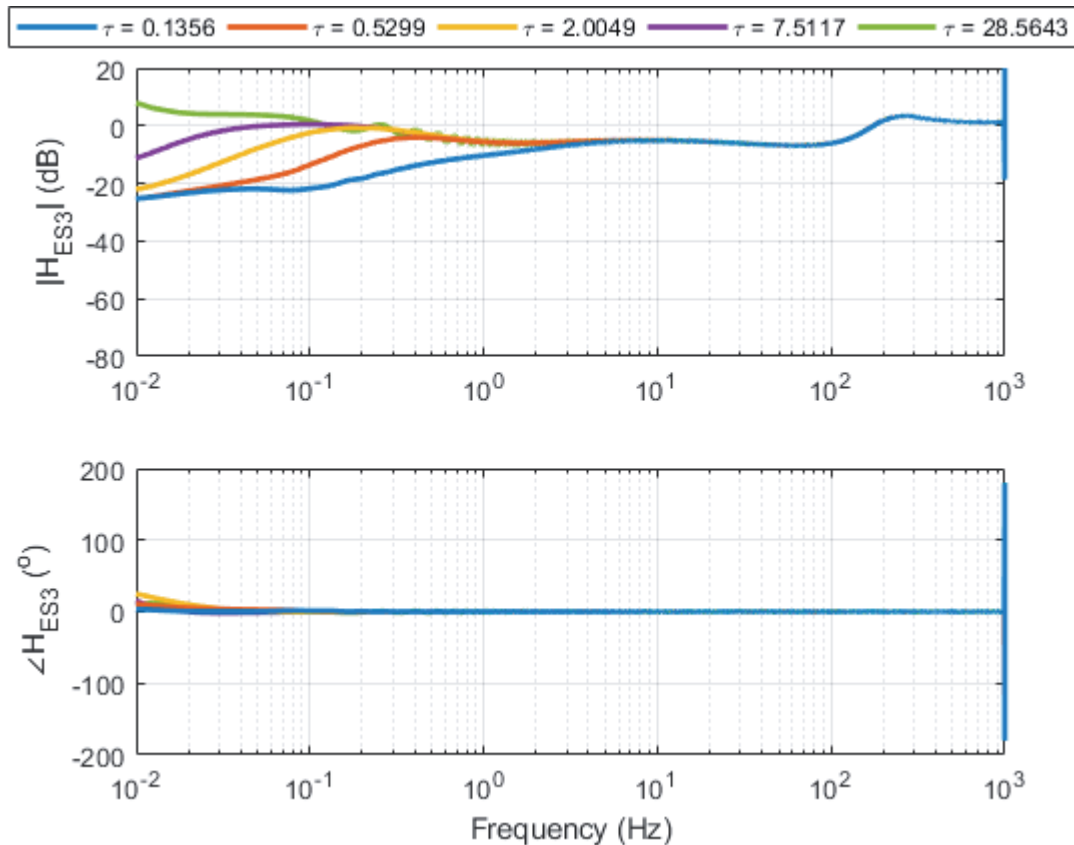


Figure 13: Transfer Function between the Grid 3 Energy Storage and the Grid 3 Load

#### 4. Conclusions

To determine energy storage requirements for the power system, analysis of the microgrid was performed with various control strategies and operational loads. Using the information acquired by this analysis, requirements for

the energy storage system in terms of the specific energy and power densities of the system were found. These requirements were applied to a Ragone plot to determine the best energy storage technology for the application (Byrne, 2007). The simulation results show that a flywheel storage technology would most effectively meet the energy and power requirements of a potential scenario with a reasonable size of 3000 kg. However, when examining the system's frequency behaviour it can be shown that this technological solution may not be able to supply the necessary frequency content that some pulsed loads will require. This result calls for a hybrid energy storage solution that could combine the advantages of multiple different technologies. Future work includes the optimisation of a hybrid energy storage design to meet the power demands of such a system.

## 5. Acknowledgements

This work was supported by NAVSEA for a project entitled *Nonlinear Power Flow Control Design for NGIP Energy Storage Requirements*, PR# 1400354102.

The authors also wish to thank Forest White, Todd Hendrickson, Mike Horry, and John Brown for their contributions to the hardware testbed.

Sandia National Laboratories is a multi-mission laboratory managed and operated by National Technology and Engineering Solutions of Sandia, LLC., a wholly owned subsidiary of Honeywell International, Inc., for the U.S. Department of Energy's National Nuclear Security Administration under contract DE-NA0003525.

The views expressed in the article do not necessarily represent the views of the U.S. Department of Energy or the United States Government.

This paper was approved under SAND number SAND2018-5938 C.

## 6. References

R. J. Allen, C. N. Boyer, B. M. Huhman, J. M. Neri and M. J. Veracka, "Progress Toward a Self-Contained Rapid Capacitor Charger for a Small Railgun in Burst Mode Operation at 3 RPS," Power Modulator and High Voltage Conference (IPMHVC), 2012 IEEE International, pp. 218-220, June 3-7, 2012.

J. S. Bernardes, G. P. LaCava and M. J. Schrader, "Analysis of a Railgun Capacitor-Muzzle-Shunt Energy Recovery Scheme," Power Modulator Symposium, 2002 and 2002 High-Voltage Workshop. Conference Record of the Twenty-Fifth International, pp. 347-350, June 20- July 3, 2002.

R. H. Byrne, J. C. Neely, S. Buerger, J. T. Feddema, D. K. Novick, S. E. Rose, B. L. Spletzer, B. R. Sturgis and D. G. Wilson, "Advanced Robot Locomotion," SAND2007-1466, Albuquerque, NM, 2007.

A.M. Cramer, X. Liu, Y. Zhang, J. D. Stevens and E. L. Zivi, "Early-stage shipboard power system simulation of operational vignettes for dependability assessment," *2015 IEEE Electric Ship Technologies Symposium (ESTS)*, Alexandria, VA, 2015, pp. 382-387.

J. S. Chalfant and C. Chryssostomidis, "Analysis of Various All-Electric-Ship Electrical Distribution System Topologies," 2015 IEEE Electric Ship Technologies symposium, ESTS 2015, Old Town Alexandria, VA, June 21-24, 2015.

N. Doerry, Next Generation Integrated Power System NGIPS Technology Development Roadmap, Washington, D. C. : Naval Sea Command, Ser. 05D/349, November 2007.

S. W. Ferguson, R. Stever, A. Throop, B. Felker and R. Franklin, "MTX/ELF II microwave power measurements and calibration for the 2 GW, 140 GHz, ELF II free-electron laser," Fusion Engineering, 1989. Proceedings, IEEE Thirteenth Symposium on, vol. 1, pp. 145-148, October 2-6, 1989.

J. Kuseian, "Naval Power Systems Technology Development Roadmap PMS 320," Naval Sea Systems Command, Washington, D. C., April 2013.

J. Neely, L. Rashkin, M. Cook, D. Wilson and S. Glover, "Evaluation of Power Flow Control for an All-Electric Warship Power System with Pulsed Load Applications," in APEC 2106, Long Beach Convention & Entertainment Center, Long Beach, CA, 2016.

C. G. Parazzoli, R. E. Rodenburg, J. B. Romero, J. L. Adamski, D. J. Pistorsei, D. R. Shoffstall and D. Quimby, "CW 100 kW radio frequency-free-electron laser design at 10  $\mu\text{m}$ ," Quantum Electronics, IEEE Journal of , vol. 27, no. 12, pp. 2605-2612, December 1991.

R. K. Pitman, R. L. Ellis and J. S. Bernardes, "Iterative Transient Model for Railgun Electro-Mechanical Performance Optimization," 12th Symposium on Electromagnetic Launch Technology, pp. 96-99, May 25-28, 2005.

A. Riccobono and E. Santi, "Comprehensive review of stability criteria for DC power distribution systems," IEEE Transactions on Industry Applications, vol. 50, pp. 3525-3535, 2014.

R. D. Robinett III and D. G. Wilson, Nonlinear Power Flow Control Design: Utilizing Exergy, Entropy, Static and Dynamic Stability, and Lyapunov Analysis, London: Springer-Verlag London Ltd. , August 2011, ISBN 978-0-85729-822-5.

R. D. Robinett III and S. G. Glover, "Enabling Secure Scalable Microgrids with High Penetration Renewables," Grand Challenge, LDRD, Sandia Technical Report, SAND2011-0935P, 2011.

J. Snoussi, S. Ben Elghali, R. Outbib and M. F. Mimouni, "Sliding Mode Control for frequency-based energy management strategy of hybrid Storage System in vehicular application," 2016 International Symposium on Power Electronics, Electrical Drives, Automation and Motion (SPEEDAM), Anacapri, 2016, pp. 1109-1114.

J. D. Stevens, D. F. Opila, A. M. Cramer and E. L. Zivi, "Operational Vignett-based Electric Warship Load Demand," IEEE Electric Ship Technologies symposium, ESTS 2015, Old Town Alexandria, VA, June 21-24, 2015.

Calnetix Technologies, "VYCON Direct Connect (VDC) Kinetic Energy Storage Systems: The Optimal UPS Energy Storage Solution for Mission-Critical Power Protection," VYCON datasheet, June 2015.

W. W. Weaver, R. Robinett III, G. Parker and D. Wilson, "Hamiltonian Modeling and Control of AC Microgrids with Spinning Machines and Inverters," International Symposium on Power Electronics, Electrical Drives, Automation and Motion, SPEEDAM 2016, Anacapri, Capri Island, Italy. 2016.

W. Weaver, R. D. Robinett III, G. G. Parker and D. G. Wilson, "Energy Storage Requirements of DC Microgrids with High Penetration Renewables Under Droop Control," International Journal of Electrical Power and Energy Systems, vol. 68, pp. 203-209, 2015.

W. Weaver, R. Robinett III, G. Parker and D. Wilson, "Distributed Control and Energy Storage Requirements of Networked DC Microgrids," Control Engineering Practice, vol. 44, pp. 10-19, 2015.

D. Wilson, M. A. Cook, J. Neely, S. F. Glover and L. Rashkin, "Nonlinear Power Flow Control Design for NGIPS Energy Storage Requirements, Phase I," Sandia Report SAND2016-1873, February 2016 revised.

D. Wilson, R. Robinett III and S. Goldsmith, "Renewable Energy Microgrid Control with Energy Storage Integration," 21st SPEEDAM 2012, Sorrent, Italy, June 20-22, 2012.

D. G. Wilson, J. Neely, M. Cook, S. Glover, J. Young and R. D. Robinett III, "Hamiltonian Control Design for DC Microgrids with Stochastic Sources and Loads with Applications," SPEEDAM 2014, Ishcia, Italy, SAND2014-15152PE, 2014.

D. G. Wilson and R. D. Robinett III, "Computing an Operating Parameter of a Unified Power Flow Controller". United States Patent 8930034, 6 January 2015.

D. Wilson, R. Robinett III and S. Goldsmith, "Renewable Energy Microgrid Control with Energy Storage Integration," 21st SPEEDAM 2012, Sorrent, Italy, June 20-22, 2012.

D. Wilson, R. Robinett III, W. Weaver, R. Byrne and J. Young, "Nonlinear Power Flow Control Design of High Penetration Renewable Sources for AC Inverter Based Microgrids," in International Symposium on Power Electronics, Electrical Drives, Automation and Motion. SPEEDAM 2016, Anacapri, Capri Island, Italy, 2016.